Chapter

Multi-Physics Simulation Platform and Multi-Layer Metal Technology for CMOS-MEMS Accelerometer with Gold Proof Mass

Katsuyuki Machida, Toshifumi Konishi, Daisuke Yamane, Hiroshi Toshiyoshi and Hiroyuki Ito

Abstract

This chapter describes technical features and solutions to realize a highly sensitive CMOS-MEMS accelerometer with gold proof mass. The multi-physics simulation platform for designing the CMOS-MEMS device has been developed to understand simultaneously both mechanical and electrical behaviors of MEMS stacked on LSI. MEMS accelerometer fabrication process is established by the multi-layer metal technology, which consists of the gold electroplating and the photo-sensitive polyimide film. The proposed MEMS accelerometers are fabricated and evaluated to verify the effectiveness of the proposed techniques regarding sub-1G MEMS and arrayed MEMS devices. The experimental results show that the Brownian noise of the sub-1G MEMS accelerometer can achieve 780 nG/(Hz)$^{1/2}$ and the arrayed MEMS accelerometer has a wide detection, ranging from 1.0 to 20 G. Moreover, using the developed simulation platform, we demonstrate the proposed capacitive CMOS-MEMS accelerometer implemented by the multi-layer metal technology. In conclusion, it is confirmed that the multi-physics simulation platform and the multi-layer metal technology for the CMOS-MEMS device have a potential to realize a nano-gravity sensing technology.

Keywords: MEMS accelerometer, CMOS-MEMS, multi-physics simulation, gold proof mass, multi-layer metal technology

1. Introduction

Microelectromechanical systems (MEMS) capacitive accelerometers have been widely used in application fields such as mobile devices, air bag ignition for vehicles, and vital sign monitoring systems [1–10]. Also, in the progress of the attractive Internet of the Thing (IoT) technology, MEMS accelerometers have played an important role in key devices. Recently, for several applications such as activities monitoring or the integrated inertial measurement unit (IMU), the accurate sensing devices below 1 G (G = 9.8 m/s^2) have been researched and developed regarding various types of MEMS capacitive accelerometer, while conventional MEMS accelerometers have an ability of sensing about 1 G or over several *G*'s. The performance

of the MEMS capacitive accelerometer can be determined by Brownian noise (B_N) that is inversely proportional to the mass of the proof mass. **Figure 1** shows the transition of B_N of the reported MEMS accelerometers. In order to establish a micro-gravity sensing technology based on silicon bulk or surface micromachining technologies, various types of MEMS capacitive accelerometer and complementary metal-oxide semiconductor (CMOS)–MEMS accelerometer have been reported [11–22]. We have developed the MEMS accelerometer and also added the data of our miniaturized sub-1G MEMS capacitive accelerometer [23] to this figure. The proof mass area of our device is nearly one-tenth of a silicon proof mass area size. As a result, in terms of the technological trend, it is suggested that this research and development would be continuing toward a nano-gravity sensing.

On the other hand, the above applications require the devices, which have a wide detectable range of acceleration, small size, and low power consumption. In fact, there are many difficulties in making the devices because the large size of the proof mass makes the device size larger, and also the accelerometer chip is usually combined with the LSI chips on the assembly board. In order to overcome these technical barriers, we have proposed a CMOS-MEMS accelerometer that implements a MEMS on CMOS-LSI [24, 25]. **Figure 2** shows prospects and challenges of the CMOS-MEMS technology from the view point of CMOS-LSI. It indicates that this technology has a solution of the difficulties in developing high functional devices. Especially, digital micro mirror device (DMD) is well-known as a successful example of MEMS business. The technology has the features of high functionality, high accuracy, and mass production. Thus, we have developed the multi-layer metal technology that consists of gold electroplating and sacrificial layer formation using thick polyimide film. Its features include the suitability to realize the various MEMS structures and the post-CMOS processes, which does not degrade CMOS device because the process temperature is below 310°C. Using the multi-layer metal technology, MEMS devices on CMOS LSI have been fabricated [26, 27].

Moreover, to facilitate the design of the CMOS-MEMS devices, we have researched and proposed a multi-physics simulation technique to develop such CMOS-MEMS devices using an electrical circuit simulator with a Verilog-A compatible hardware description language (HDL) for equivalent circuit description

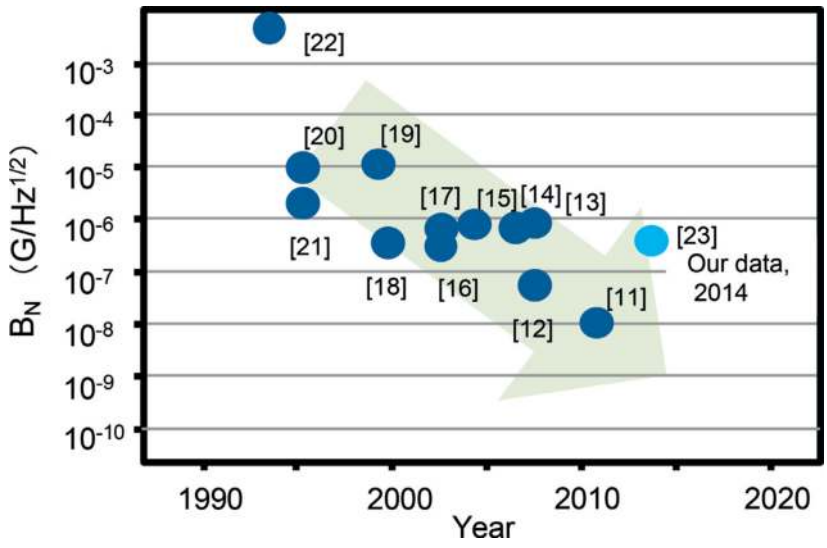

Figure 1.
The transition of the B_N of the reported MEMS accelerometers.

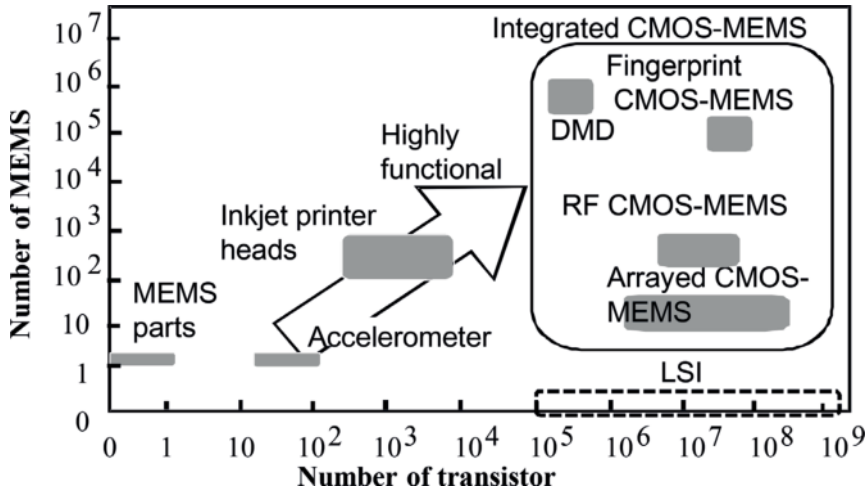

Figure 2.
Business trend and correlation between the number of MEMS devices and transistors.

[28, 29]. Thus, we have developed a capacitive CMOS-MEMS sensor designed by our multi-physics simulation. The developed sensor shows that the capacitive MEMS device is implemented on the sensor LSI [30].

In this chapter, first, the multi-physics simulation platform for the CMOS-MEMS technology is presented. Next, we describe the newly developed sensor structure and the multi-layer metal technology, which can be compatible with post-CMOS process. Third, the sub-1G MEMS accelerometer is described. Fourth, the arrayed MEMS accelerometer for wide range detection is demonstrated. Fifth, we then show the proposed sensor circuit using our multi-physics simulation environment. Finally, we demonstrate the evaluation results of the fabricated CMOS-MEMS accelerometer by the multi-layer metal technology.

2. The multi-physics simulation

2.1 Analytical model for MEMS accelerometer

Figure 3 shows a diagram of an analytical model for the MEMS accelerometer. The electrostatic capacitive MEMS accelerometer basically consists of the upper electrode of a proof mass and the bottom plate of the fixed electrode. The upper plate is supported by the spring connected to the mechanical anchor. When the proof mass detects an input acceleration in the vertical direction, the electrical capacitance between the upper and the bottom plates is modulated. The fixed electrode is applied by the input voltage V to measure the capacitance change. The analytical model includes the capacitances of C_1, C_2, and C_{air} as shown in **Figure 3**. The capacitance of C_{total} can be obtained as the following equations:

$$C_1 = \frac{\varepsilon_0 \varepsilon_1 S_1}{t_i} \tag{1}$$

$$C_2 = \frac{\varepsilon_0 \varepsilon_2 S_1}{gini - x} \tag{2}$$

$$C_{air} = \frac{\varepsilon_0 \varepsilon_2 (S_2 - S_1)}{gini - x + t_i} \tag{3}$$

$$C_{total} = C_{air} + \left(\frac{1}{C_1} + \frac{1}{C_2} \right)^{-1} = \frac{\varepsilon_2 \varepsilon_0 (S_2 - S_1)}{gini - x + t_i} + \frac{\varepsilon_0 S_1}{\frac{t_i}{\varepsilon_1} + \frac{(gini - x)}{\varepsilon_2}} \tag{4}$$

where ε_0 is the permittivity of vacuum, ε_1 is the relative permittivity of the SiO_2, ε_2 is the relative permittivity of the air, S_1 is the areas of the SiO_2 coverage, S_2 is the total areas of the movable electrode, t_i is the thickness of the SiO_2, gini is the initial air gap, and x is the displacement of the proof mass.

The input force due to the acceleration F*acc*, the mechanical viscoelastic force F*m*, the electrostatic attractive force Fe, and the relationship of their contributions is expressed in the following equations:

$$F_{acc} = 9.8mG \ , \tag{5}$$

$$F_s = kx + cx \tag{6}$$

$$F_e = \frac{1}{2} \frac{\partial C}{\partial x} V^2 = \frac{V^2}{2} \left\{ \frac{\varepsilon_2 \varepsilon_0 (S_2 - S_1)}{(gini - x + ti)^2} + \frac{\varepsilon_0 S_1}{\varepsilon_2 \left(\frac{t_i}{\varepsilon_1} + \frac{gini - x}{\varepsilon_2} \right)^2} \right\} \tag{7}$$

$$F_{acc} + F_e + F_s = 0 \tag{8}$$

where m is the proof mass, Gin is the input acceleration value measured in gravitational acceleration, k is the spring constant, and c is the damping coefficient including the viscosity of the air.

2.2 Equivalent circuit model for MEMS accelerometer

Figure 4 shows the equivalent circuit for the MEMS accelerometer implemented in Cadence Virtuoso [31], which is widely used for LSI design.

According to the Eqs. (1)–(8), we have proposed equivalent circuit of five modules:

Module (I) represents the acceleration to provide an eternal force system.

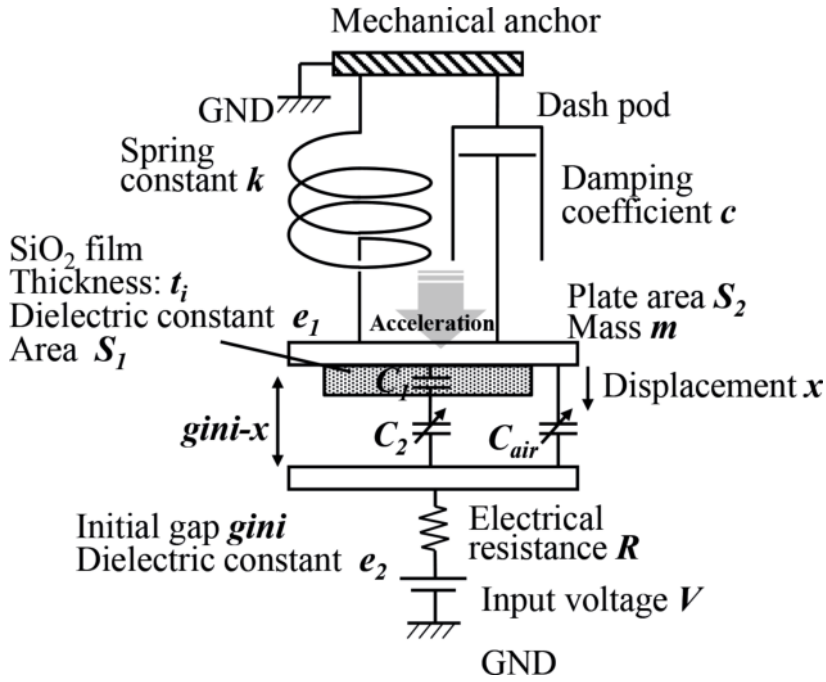

Figure 3.
Analytical model for electrostatic MEMS accelerometer.

Module (II) is the parallel-plate electrostatic actuator to calculate the electrostatic attractive force and inductive charge as a function of the applied voltages.
Module (III) is the viscoelastic suspension module.
Module (IV) is the core of the equivalent circuit, where the equation of motion (EOM) is carried out under conditions of force applied to the mass m.
Module (V) represents the mechanical anchor.

These modules are described in a Verilog-A compatible HDL. We also have established modules (I) and (II) by extending our previous work reported elsewhere [29]; likewise, modules (III), (IV), and (V) are interpreted using Eqs. (6) and (8). Meandering suspensions are used in this chapter to lower the elastic rigidity in the direction normal to the chip surface.

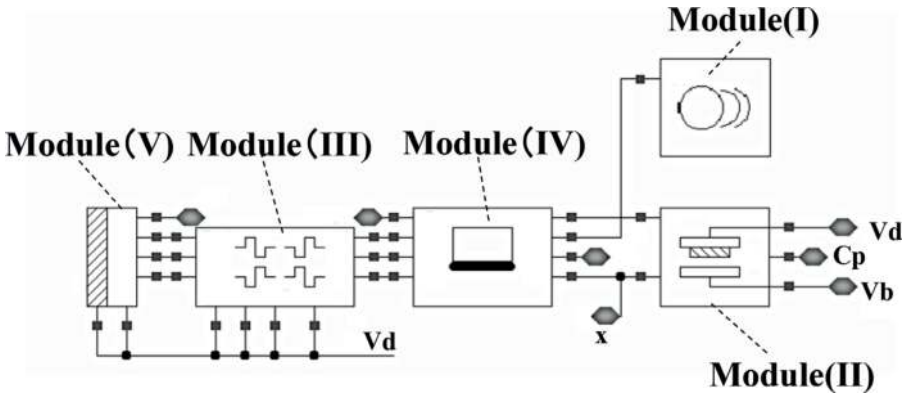

Figure 4.
Schematic image of the proposed equivalent circuits for a single MEMS accelerometer.

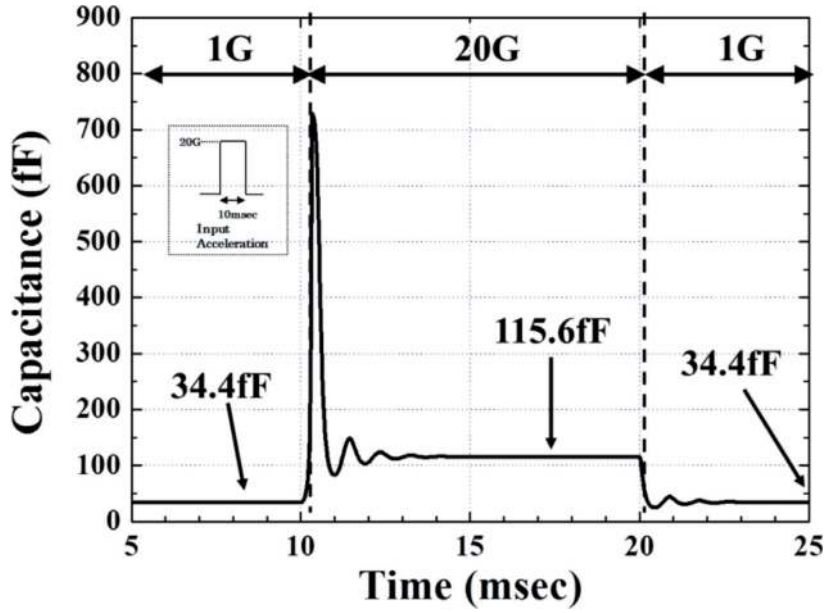

Figure 5.
Simulation results of a single MEMS accelerometer.

For verification, we performed simulation. Thus, we applied the simulation to a single MEMS accelerometer to detect a 20 G using the above equivalent circuit. **Figure 5** shows the simulation results of a capacitance change of the MEMS accelerometer under the condition of 20 G at the period of 10 ms. The result suggests that the accelerometer can detect the capacitance change without stiction. From these results, it can be concluded that the equivalent circuit would quantitatively represent the device in this chapter.

3. MEMS accelerometer

3.1 Accelerometer structure

Figure 6 shows the concept of the proposed MEMS accelerometer structure, which is composed of the movable proof mass, the fixed bottom electrode, stopper,

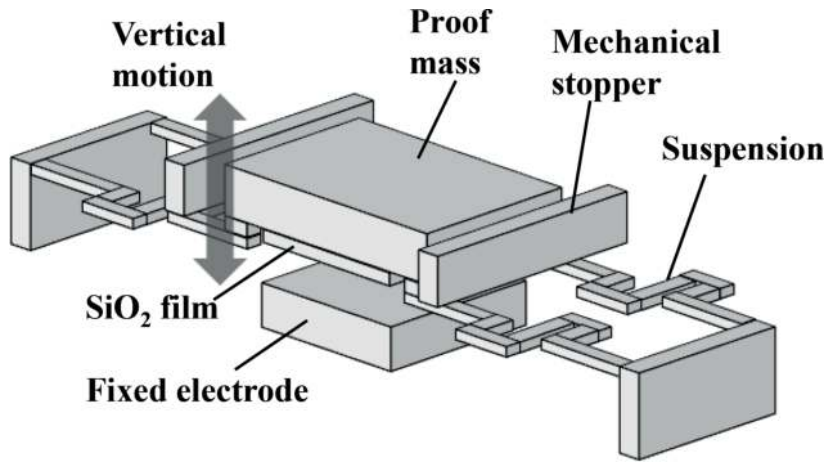

Figure 6.
The conceptual image of the proposed MEMS sensor structure.

and suspension. The accelerometer structure has the following three features; (i) in order to facilitate flexibilities of design, we have utilized the multi-layer metal technology [12, 32–34]. The multi-layer metal technology can adjust the weight of the proof mass and the spring constant of mechanical suspensions, (ii) the stopper structure is built to prevent mechanical destruction from lateral and vertical over-swings of the proof mass, and (iii) the SiO_2 film is formed to prevent sticking and electrical short between the proof mass and the fixed electrode.

3.2 Proof mass material

The proof mass size should be substantially reduced while keeping adequate weight on it, we can then downscale the sensor area without compromising the sensitivity. The minimum detection sensitivity of the accelerometer is limited by Brownian noise (B_N) as described in the following equation [19]:

$$B_N = \frac{\sqrt{4k_B Tb}}{m} \tag{9}$$

where T, b, k_B, and m are the absolute temperature, the viscous damping coefficient, the Boltzmann constant (1.38×10^{-23} J/K), the absolute temperature, and the proof mass of an accelerometer, respectively. We have searched the suitable materials for the proof mass to further minimize B_N. **Figure 7** shows the comparison of the Brownian noise on the proof masses made of different types of materials. Our target value of the B_N can be below 100 μG/(Hz)$^{1/2}$ to provide a sufficiently low Brownian noise [24, 25] for a practical use. Thus, gold could be a candidate material for small proof mass size. In addition, gold material should also be suitable for the fabrication process of the CMOS-MEMS accelerometer that gold electroplating has successfully stacked MEMS on an LSI circuit [26, 35, 36].

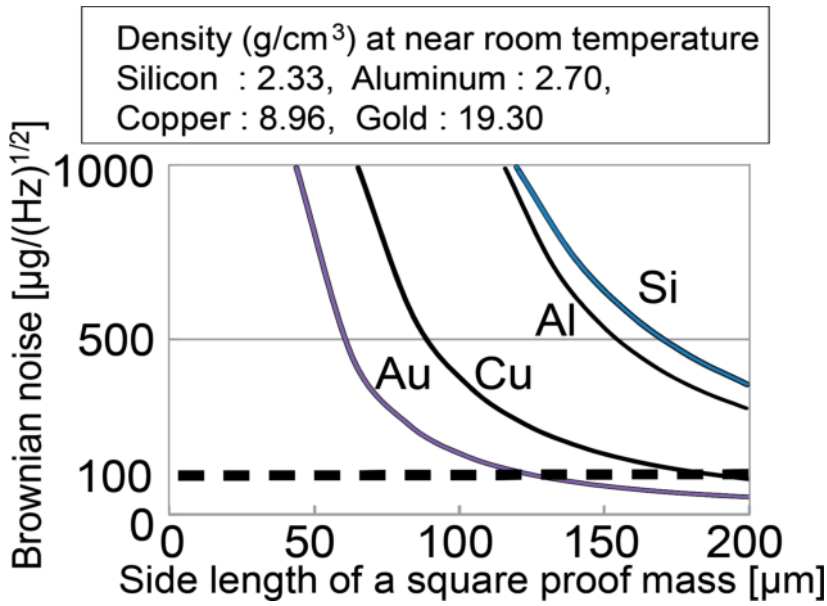

Figure 7.
The comparison of the Brownian noise on the proof masses.

3.3 Fabrication process

Figure 8 shows the fabrication process flow for the designed MEMS accelerometer. Firstly, Ti/Au adhesion and seed layers were deposited by the vacuum evaporation on a thermal SiO_2 (**Figure 8a**). After forming the electrodes and interconnections using the patterning process, photo-sensitive polyimide film was then spin-coated and annealed at 310°C as a first sacrificial layer. The gold electroplating formed the bottom gold layer (**Figure 8b**); this metallization was applied in every metal layer process as described in the following. After depositing next sacrificial layer of photo-sensitive polyimide film supporting gold of the thickness of 3 μm (**Figure 8c**), contact holes for interconnections were made, and then a 0.5 μm thick SiO_2 was deposited by sputtering (**Figure 8d**). Finally, the proof mass and stopper structures 15 μm in thickness were formed on the uppermost gold (**Figure 8e**) followed by removing all sacrificial films by oxygen plasma etching (**Figure 8f**). Thus, this fabrication process is compatible with CMOS-LSI due to the control of the process temperature below 400°C.

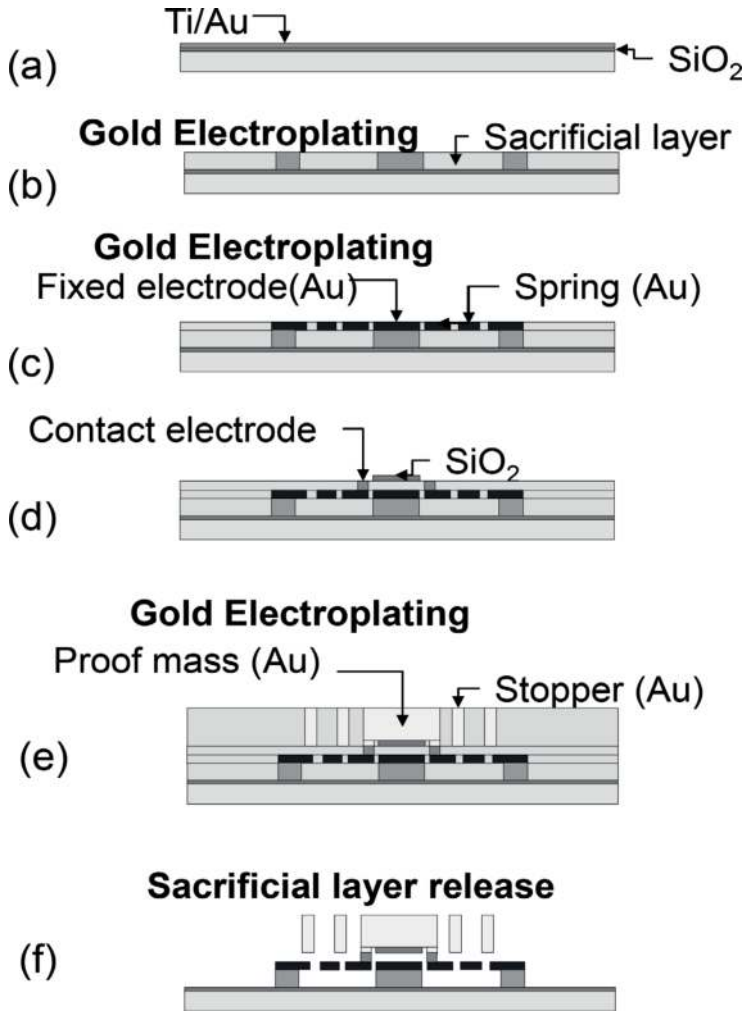

Figure 8.
The micro-fabrication flow for the designed MEMS accelerometer. (a) adhesion and seed layers formation. (b) first metal and sacrificial film formation. (c) second metal formation. (d) contact metal and SiO_2 formation. (e) Proof mass and stopper formation. (f) Final process.

3.4 Experimental results of MEMS accelerometer

Figure 9 shows the SEM micrograph of the MEMS accelerometer, which has been successfully developed through the proposed fabrication process. We show the evaluation results of the measured characteristics of the developed MEMS accelerometer. **Figure 10** shows the capacitance vs. voltage characteristics were measured and plotted by applying a direct-current voltage between the movable proof mass and the fixed electrodes without applying acceleration. The initial capacitance C_0 at a voltage of 0 V, the electrostatic pull-in at a voltage of 6.4 V, and the release operation without stiction failure were observed from the hysteresis curve in **Figure 10**. The actual initial gap and spring constant have been estimated to be 4.3 μm and 0.26 N/m, respectively, in good agreement with the designed values. **Figure 11** shows the capacitance vs. frequency characteristics under the condition of a bias voltage of 2 V with 100 mV-amplitude oscillation. The measured

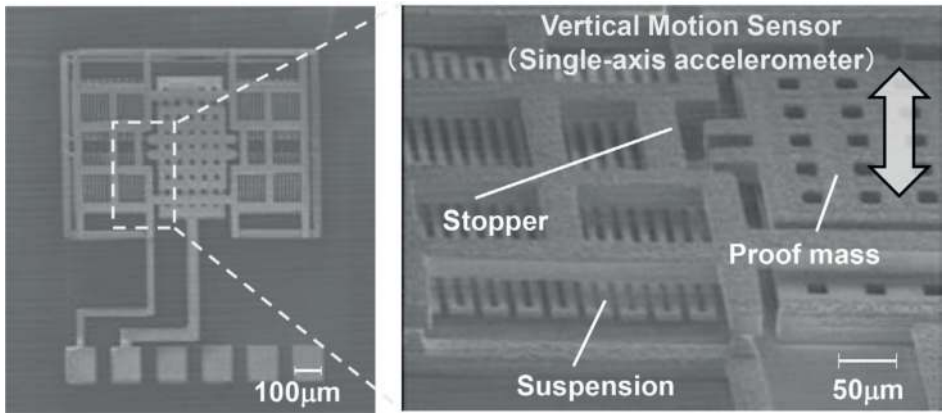

Figure 9.
The SEM micrograph of the MEMS accelerometer.

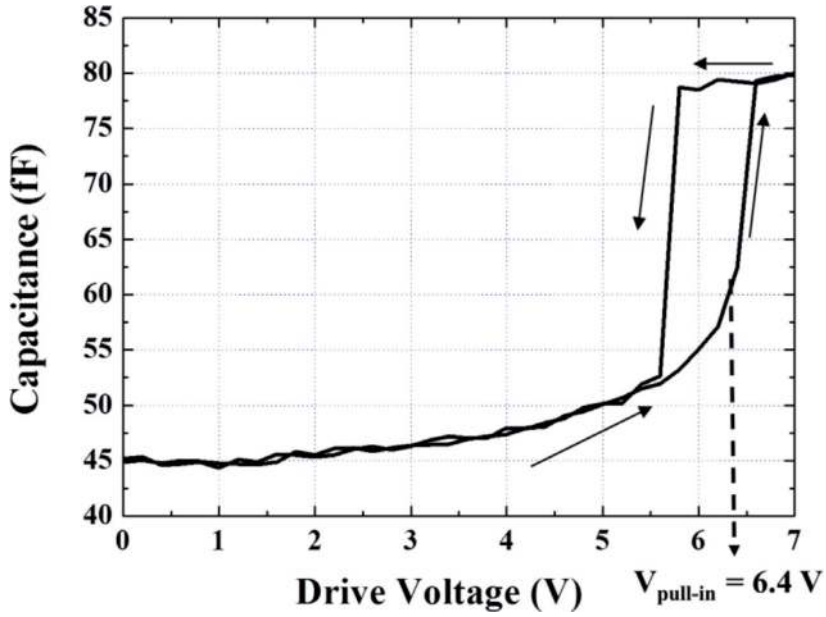

Figure 10.
The capacitance vs. voltage characteristics.

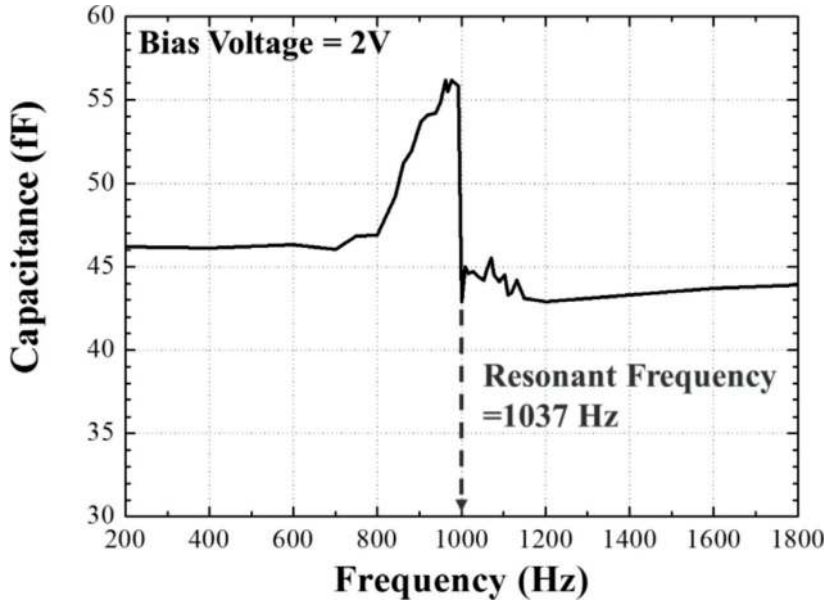

Figure 11.
The capacitance vs. frequency characteristics.

mechanical resonant frequency showed approximately 1037 Hz. The result suggested that it was higher than the designed value of 687 Hz due to the difference between the actual and the designed spring constants.

Figure 12 shows the capacitance vs. the applied acceleration characteristics. We measured the capacitance value at a bias voltage of 2 V with a frequency of 50 Hz. The measured results and the calculated data were square dots and the solid line, respectively. The calculated data used the actual proof mass of 6.12×10^{-9} kg. The designed proof mass was 1.07×10^{-8} kg. The result indicated that the experimental data was coincident with the calculated data.

Table 1 shows the comparison of the design and the obtained parameter values. The measured spring constant of 0.26 N/m is higher than the designed value of 0.2 N/m. The Brownian noise was measured to be 90.6 μG/(Hz)$^{1/2}$ for a proof mass

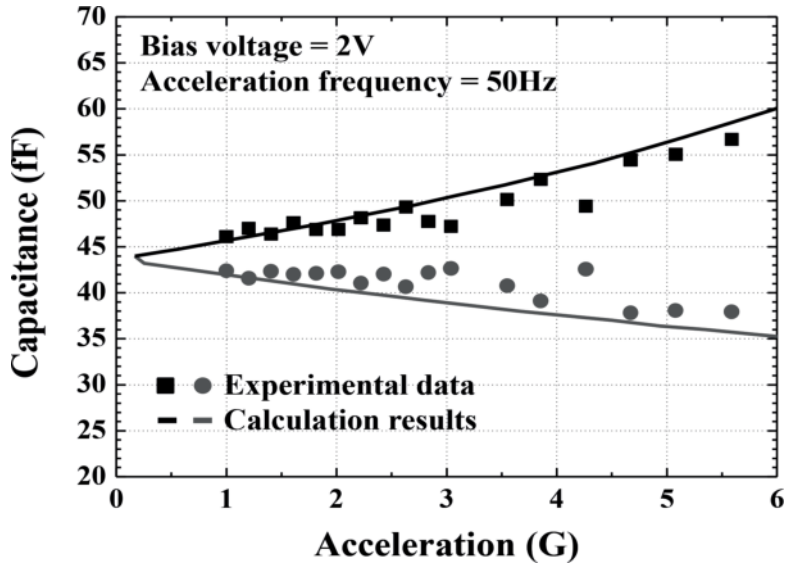

Figure 12.
The capacitance vs. the applied acceleration characteristics.

Parameter	Design Value	Measured	Unit
Initial Gap	5.0	4.3	μm
Pull-in Voltage	6.0	6.4	V
Spring Constant	0.2	0.26	N/m
Mechanical Resonant Frequency	687	1037	Hz
Q factor	2.5	2.1	-
Brownian Noise	51.6	90.6	$\mu G/(Hz)^{1/2}$
Detective Range	+/-1.7	+/-5.6	m/s^2

Table 1.
The obtained parameter values.

with a size of 140 × 140 μm^2. Thus, this result attained the target value of less than 100 $\mu G/(Hz)^{1/2}$. Therefore, these evaluation results have verified the feasibility of our proposed structure and the multi-layer metal technology utilizing gold as a material for MEMS accelerometers.

4. Sub-1G MEMS accelerometer

4.1 Design of sub-1G MEMS accelerometer

This section shows a design approach of sub-1G detectable MEMS capacitive accelerometers for the miniaturization of CMOS-MEMS inertial sensors [23]. The minimum detectable acceleration can be determined by the Brownian noise B_N. Utilizing the high-density gold proof mass, the proof mass area of our device is nearly one-tenth of a silicon proof mass area size. The MEMS capacitive accelerometer for sub-1G sensing have been designed as follows: (i) a low B_N design below 10 $\mu G/(Hz)^{1/2}$, (ii) the mechanical resonant frequency of the accelerometer higher than the frequency of common environmental vibrations, which was mostly below 100 Hz [37, 38], and (iii) the multi-layer metal technology has been employed. Moreover, the feature size of the mechanical spring was designed to avoid physical contact between the proof mass and the fixed electrode. An SiO_2 film was used on the fixed electrode to avoid stiction as shown **Figure 6**.

We proposed a sub-1G detectable MEMS capacitive accelerometer with a proof mass made of gold. The proposed MEMS accelerometer has been developed by the multi-layer metal technology reported elsewhere [26, 27]. **Figure 13** shows the scanning electron microscope (SEM) micrographs of the fabricated accelerometer. The micrographs indicate the mechanical springs, the square proof mass with numbers of release holes, and mechanical stoppers. Thus, multi-layer gold has been successfully formed; the multi-layer metal structures have realized the decreased thickness of the mechanical springs to lower the vertical spring constant for the sub-1G sensing, while increasing the proof mass for a heavy mass. The proof mass was designed to be 1020 μm × 1020 μm in area and 12 μm in thickness. From the designed result, we obtained the small value of B_N = 120 $nG/(Hz)^{1/2}$. The value was considered to be sensitive to a sub-1G acceleration at the resolution of 1 mG.

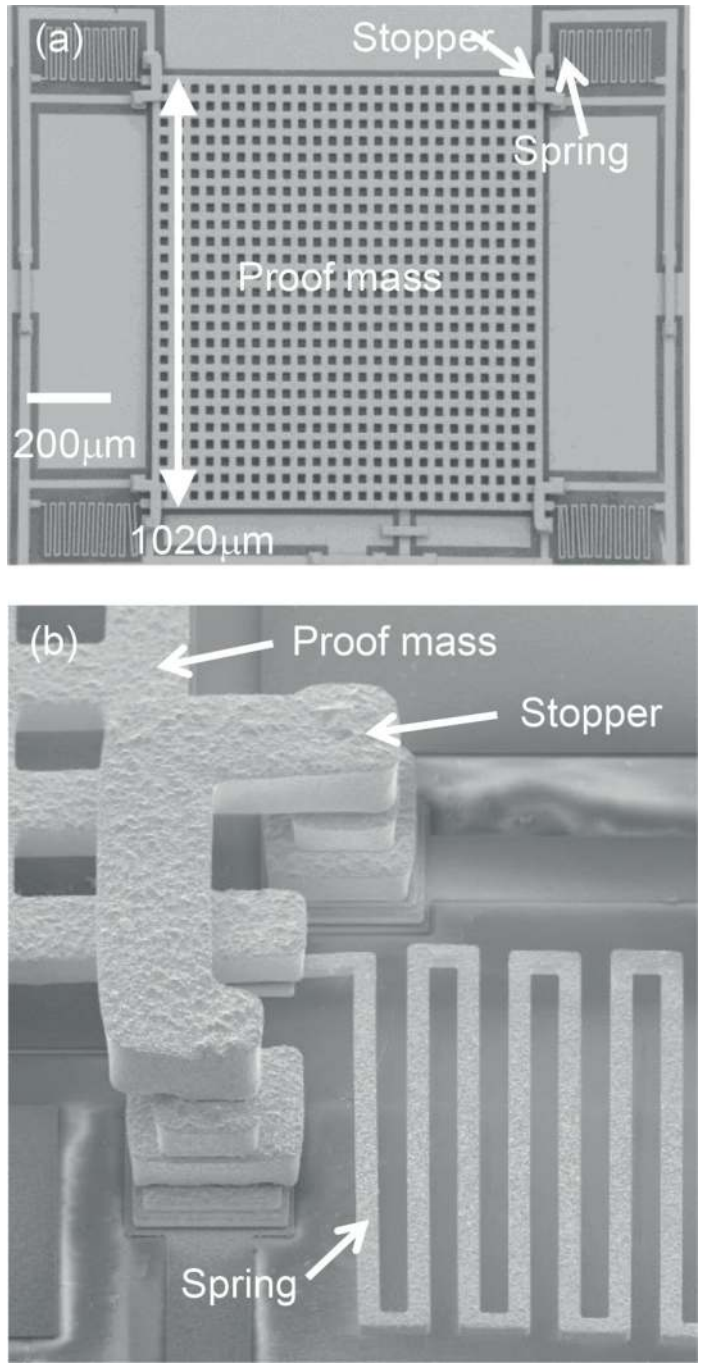

Figure 13.
SEM micrographs of a MEMS accelerometer with the squared proof mass. (a) Chip view and (b) close-up image.

The resolution was presumed by considering the root-mean-square (rms) of the acceleration noise ($a_{n,rms}$). Assuming the single-pole roll-off characteristics, the equivalent noise bandwidth (Δf) is given by [39]:

$$\Delta f = 1.57 \times f_{-3dB}, \tag{10}$$

where f_{-3dB} is the cutoff frequency, at which the output of the circuit falls −3 dB off the nominal passband level. The $a_{n,rms}$ is defined as [40]

$$a_{n,rms} = B_N \times \sqrt{\Delta f}. \tag{11}$$

For the Gaussian noise with a given rms value, the minimum detectable acceleration a_{min} can be statistically predicted by using $a_{min} = 6.6 \times a_{n,rms}$ [41]. The B_N value should satisfy the requirement of $a_{min} < 1$ mG is $B_N < 12$ μG/(Hz)$^{1/2}$ for a typical f_{-3dB} of 100 Hz. Thus, we determined the target B_N to be lower than 10 μG/(Hz)$^{1/2}$ and designed a heavy proof mass with $B_N = 120$ nG/(Hz)$^{1/2}$ to allow for safety margin. **Figure 14** shows the capacitance vs. input acceleration (gravity) characteristics. The MEMS chip was set on a vibration exciter to apply vertical accelerations of 19.9 Hz with the DC bias voltage of 1.5 V. The result suggests the accelerometer's capability of sensing a sub-1G input acceleration with a 0.1-G step. **Figure 15** shows the capacitance vs. frequency characteristics. The measurement result indicates that the mechanical resonant frequency was measured to be 777 Hz and the resonant vibration of the proof mass was higher than the frequency of common environmental vibrations (<100 Hz). The quality factor (Q) of the device was 6.40 from the C-F characteristics by calculating the ratio between the real (Z_R) and imaginary (Z_I) parts of the electrical impedance at the resonant frequency; the Z_R and Z_I are 1.97×10^7 and -1.26×10^8, respectively.

To estimate the actual value of B_N on the developed MEMS accelerometer, we use the following analytical models. The Q of a proof mass is expressed as [40]

$$Q = \frac{m\omega_{res}}{b}, \tag{12}$$

where ω_{res} is the resonant angular frequency. Using Eqs. (9) and (12), B_N can be given by

$$B_N = \sqrt{\frac{4k_B T\omega_{res}}{mQ}}. \tag{13}$$

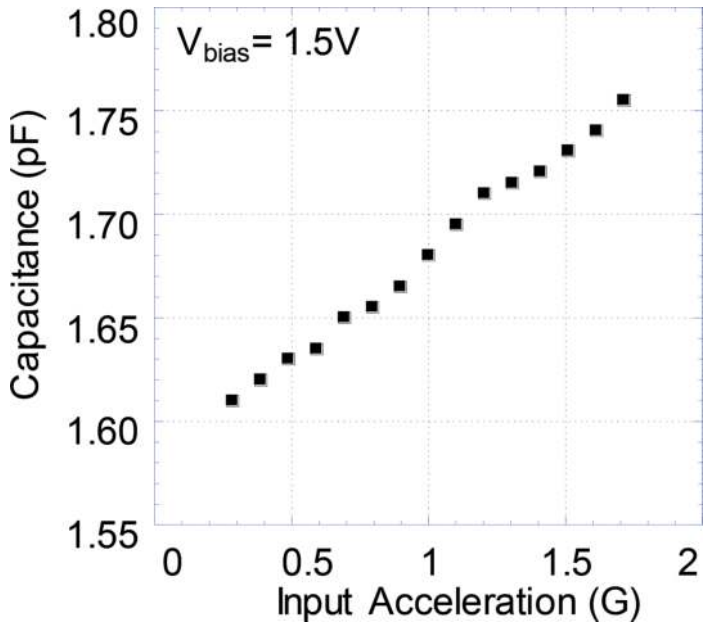

Figure 14.
Capacitance as a function of acceleration.

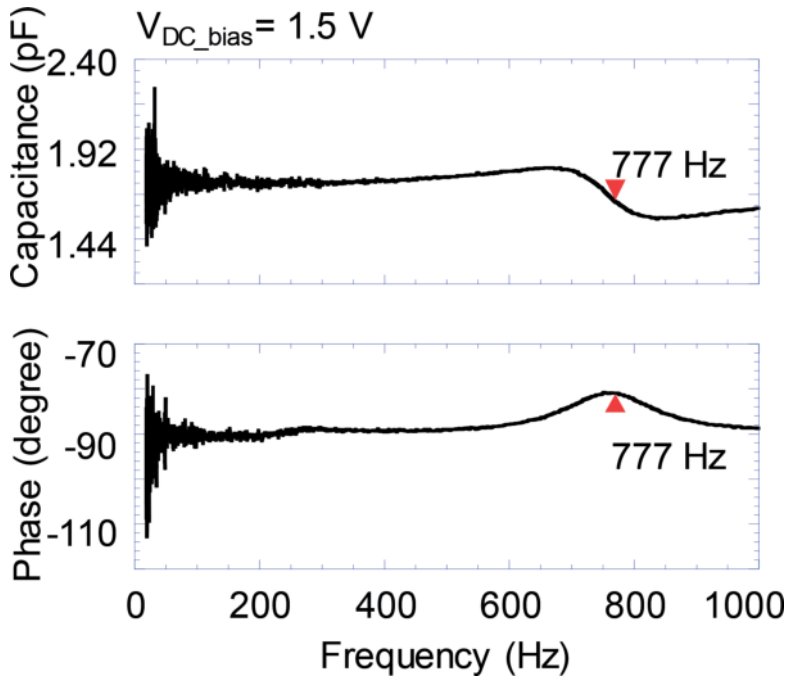

Figure 15.
Measured capacitance and phase characteristics as a function of the frequency of sensing signal.

We can obtain the B_N value by the Eq. (13) and the experimentally obtained data, when it is difficult to explain the actual value of b due to the squeezed-film damping effect [41]. Measuring the area and height of the proof mass, and the m was obtained to be 2.17×10^{-7} kg. Thus, the actual B_N can be estimated to be 780 nG/(Hz)$^{1/2}$ at 300 K, which was below the target value of 10 μG/(Hz)$^{1/2}$.

Therefore, it is confirmed that the Brownian noise of the sub-1G MEMS accelerometer can achieve 780 nG/(Hz)$^{1/2}$ in spite of the small proof mass.

5. Arrayed MEMS accelerometer

5.1 Proposed MEMS accelerometer

Figure 16 shows that an arrayed CMOS MEMS accelerometer stacked on a single LSI chip [24]. In order to solve the issues on the conventional MEMS accelerometers, the proposed accelerometer has the following requirements: (i) the accelerometer should be in an arrayed type to detect a wide range of acceleration, (ii) the structure material for the accelerometer should be chosen to reduce the sensor size and the mechanical noise floor, and (iii) the accelerometer should be stacked on the single CMOS LSI. Proof masses of three different designs (areas 80 × 80, 140 × 140, and

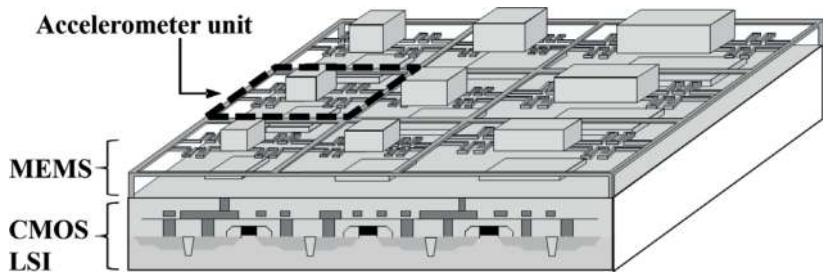

Figure 16.
An integrated CMOS-MEMS accelerometer.

200×200 μm^2) are combined with three types of different spring constants (0.2, 0.3, and 0.4 N/m) to detect the wide range of acceleration from 1 to 20 G. The total layout area is less than 4×4 mm^2, which is small enough for monolithically integration with CMOS circuits. **Figure 17** shows the calculated electrostatic capacitance as a function of the input acceleration by using the multi-physics simulation; a bias voltage of 1 V was applied to the sensing electrode for electrostatic capacitive readout. The acceleration was swept from 0 to ±20 G in 10 s for each branch. The simulation results showed that the capacitance was changed by the input acceleration within the limited mechanical displacement range between the bottom electrode and the mechanical stopper. In the positive acceleration, the capacitance gradually increases by squeezing the air gap between the proof mass and the fixed electrode. Owing to the bias voltage of 1 V, the proof mass was brought into pull-in contact. In the opposite acceleration, the air gap is enlarged to decrease the capacitance. **Figure 17** also suggests that a wide range of acceleration between 1 and 20 G is covered by the arrayed accelerometers; for instance, any one of accelerometer #2, 3, 5, 6, 8, or 9 can detect an acceleration of 3 G or greater. For a range lower than 2 G, accelerometer #3 can be used.

5.2 Results and discussion of arrayed MEMS accelerometer

Figure 18 shows a scanning electron microscopy (SEM) image of the developed MEMS accelerometers in 3×3 formation. **Figure 19** shows the measured acceleration characteristics (dots) as a function of the capacitance change compared to the simulation results. The measurement was carried out under the condition of the acceleration frequency of 50 Hz and the bias voltage of 100 mV. The simulation results include the effect of the parasitic capacitance C_{pa} of the measurement system. The measured data of devices #1, 2, 4, 5, 7, and 8 exhibited good agreement with the simulation results. On the other hand, the data of devices #3, 6, and 9 showed the capacitance change smaller than the simulation. This is because these latter three devices used a proof mass of 200×200 μm^2 size so that the mismatch might be caused by a size effect such as warpage.

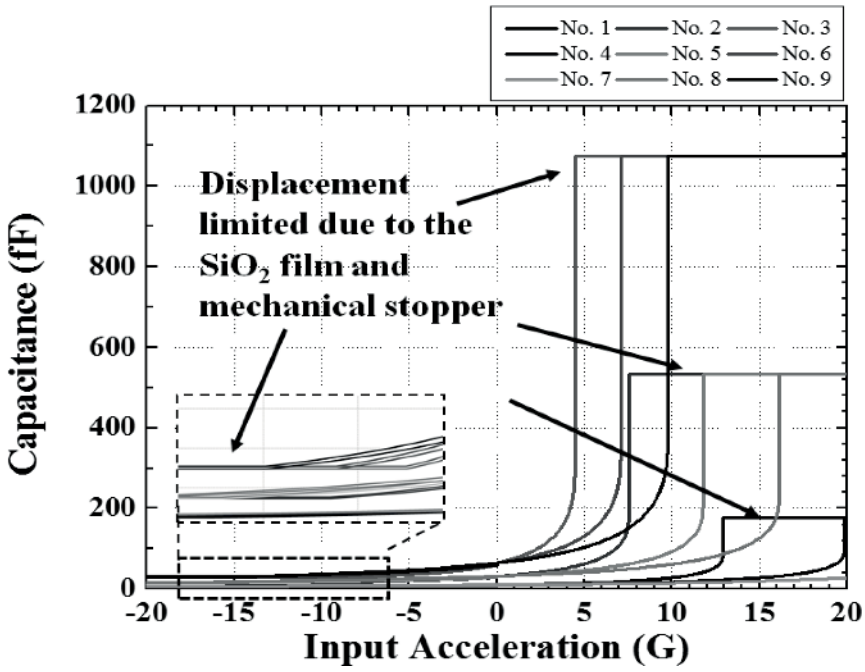

Figure 17.
The calculated electrostatic capacitance as a function of the input acceleration by using the multi-physics simulation.

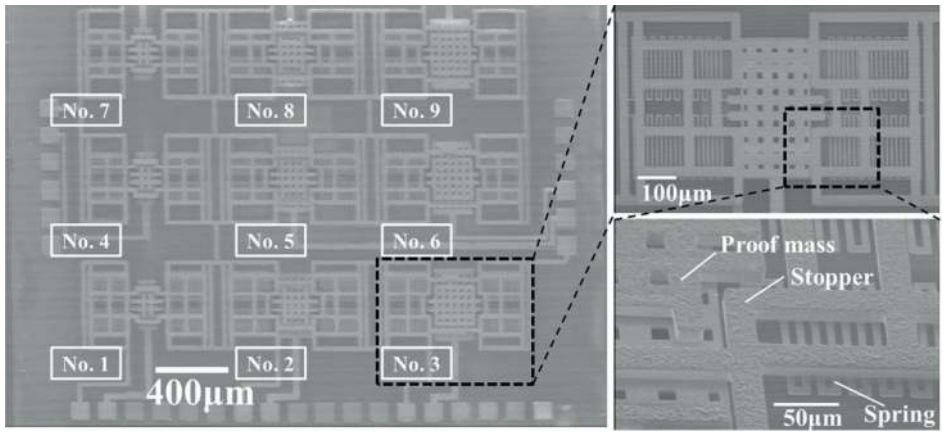

Figure 18.
A scanning electron microscopy (SEM) image of the developed MEMS accelerometers.

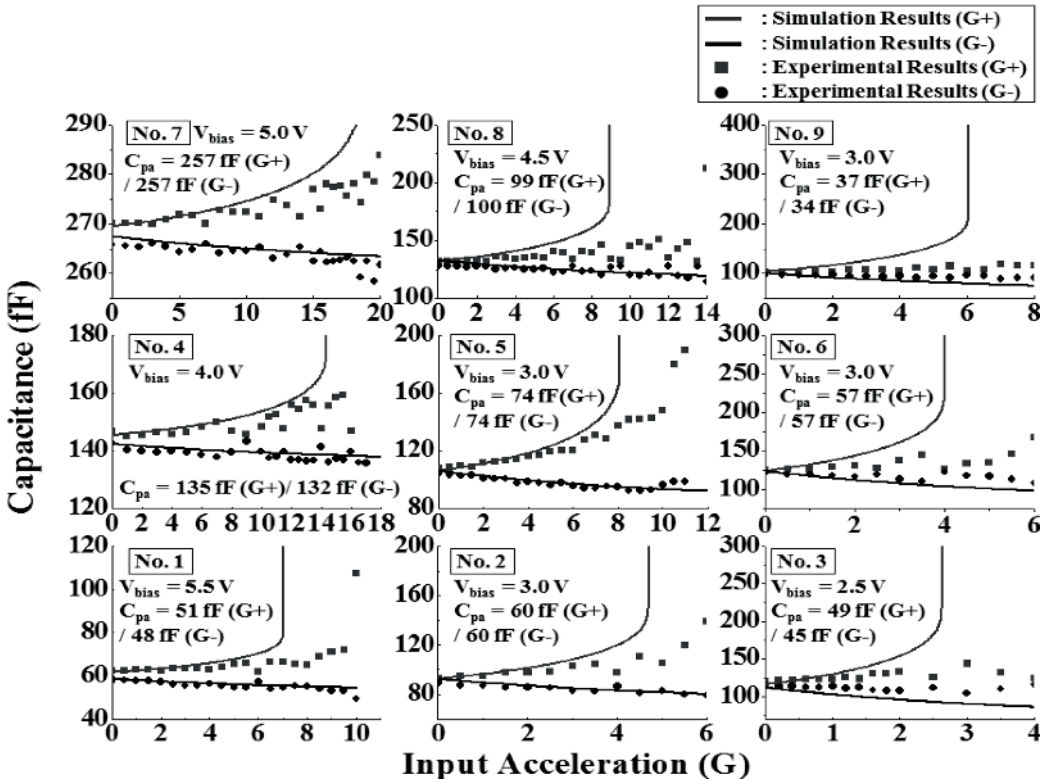

Figure 19.
The experimentally obtained acceleration characteristics.

Therefore, it is confirmed that the proposed arrayed MEMS accelerometer could detect a wide range of acceleration from 1 to 20 G.

6. CMOS-MEMS accelerometer

6.1 Capacitive CMOS sensor

In order to verify the validity of our CMOS-MEMS technology, we have developed a capacitive CMOS-MEMS accelerometer designed by our multi-physics

simulation. The developed accelerometer is composed of the capacitive sensor LSI circuit and the MEMS accelerometer. We propose the sensor circuit to detect the capacitance change of the MEMS device by comparing with the reference capacitor built-in LSI. The MEMS accelerometer and the proposed sensor circuit are simultaneously designed by the multi-physics simulation with a newly developed equivalent circuit of the capacitive MEMS sensor for CMOS-MEMS technology.

6.2 Sensor circuit

Figure 20 shows the comparison of our capacitive MEMS sensor circuit and the conventional MEMS sensor circuit. In conventional MEMS sensor circuits [42–44], capacitance change of the movable electrodes is differentially detected in response to the changes of another electrode pair within the identical MEMS chip such as the comb-drive devices. On the other hand, in our capacitive MEMS sensor circuit, it is needed to adopt other detection architecture different from the conventional sensor circuit as described above. It is because the electrode is only placed at the bottom side of the proof mass and also differential capacitance values are not produced.

In order to solve the above requirements, we propose the sensor circuit to detect a capacitance signal from a MEMS sensing element and compare it with a reference capacitor integrated within the sensor LSI. **Figure 20** shows the concept of our proposed sensor circuit. This circuit does not need other electrodes or structures for the differential capacitance. Thus, it is applicable to our capacitive CMOS-MEMS accelerometer. The circuit also has other features: (i) a reference capacitor in a MEMS chip is not needed, and hence the total device footprint is reduced, (ii) it is applicable and scalable to various types of capacitive MEMS devices including accelerometer in an arrayed format [24, 25], and (iii) calibration is simply proceeded as we can know the reference capacitor values at the stage of circuit design.

6.3 Capacitive CMOS-MEMS accelerometer design

To realize a capacitive CMOS-MEMS accelerometer, we utilized the multi-physics simulation platform based on our previous work [29]. **Figure 21** shows the proposed sensor circuit with an equivalent circuit of the capacitive MEMS accelerometer. The equivalent circuit consists of five modules. These modules are described by a Verilog-a compatible HDL, and designed to handle the multi-physics simulations in a single LSI design environment such as Cadence Virtuoso [31].

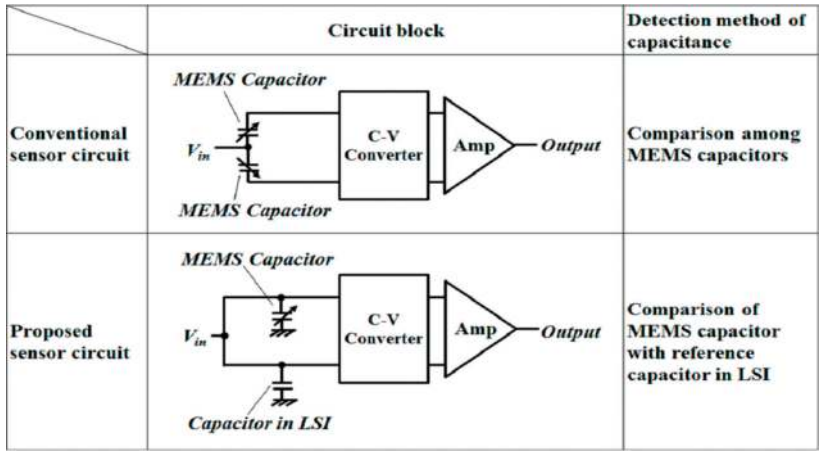

Figure 20.
The comparison of the capacitive CMOS-MEMS sensor and the conventional MEMS sensor.

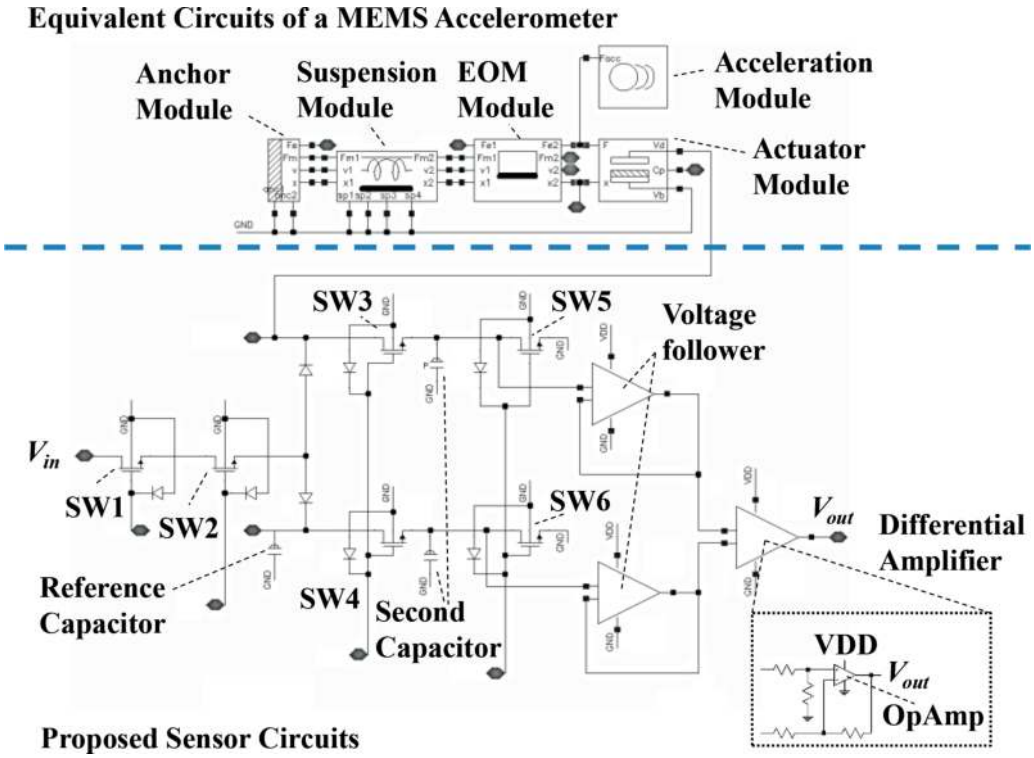

Figure 21.
The schematic of the proposed sensor circuit with an equivalent circuit of the capacitive MEMS sensor as a MEMS accelerometer.

The behaviors of both LSI and MEMS should be simultaneously simulated to design the capacitive CMOS-MEMS accelerometer stacked on the sensor circuit. Capacitance values C_{tm} and C_{tr} of the capacitor are set to be 8 pF with the parasitic capacitance of 7 pF in the LSI and the measurement system. In these parameters, we performed a transient analysis for the acceleration of sinusoidal wave of 2 G_{in} at 49 Hz superposed onto a DC level acceleration of 1 G. **Figure 22** shows the simulation results of the output voltage from the proposed sensor circuit under given input acceleration. This result suggests that the output voltage has changed from 869.3 to 892.1 mV depending upon the input acceleration waveforms.

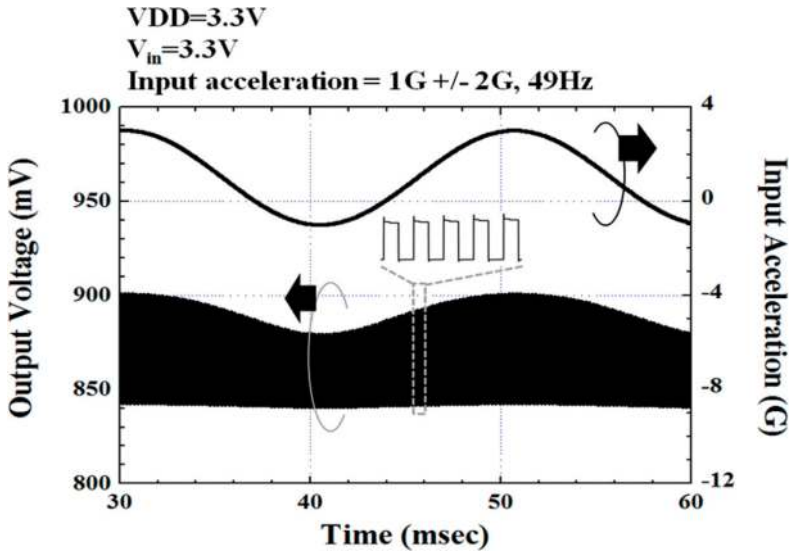

Figure 22.
The simulation results of the output voltage from the proposed sensor circuit under given input acceleration.

DOI: http://dx.doi.org/10.5772/intechopen.81832

As a result, it is confirmed that the proposed sensor circuit could detect the capacitance change of the MEMS device.

6.4 Experimental results of capacitive CMOS-MEMS accelerometer

Figure 23 shows a scanning electron microscopy (SEM) image and a close-up optical microscope view of the developed capacitive CMOS-MEMS accelerometer. It is clear that the MEMS structure interconnected to the LSI has been successfully fabricated by the micro fabrication process. **Figure 24** shows the output voltage as a function of the input acceleration obtained by both measurement and simulation.

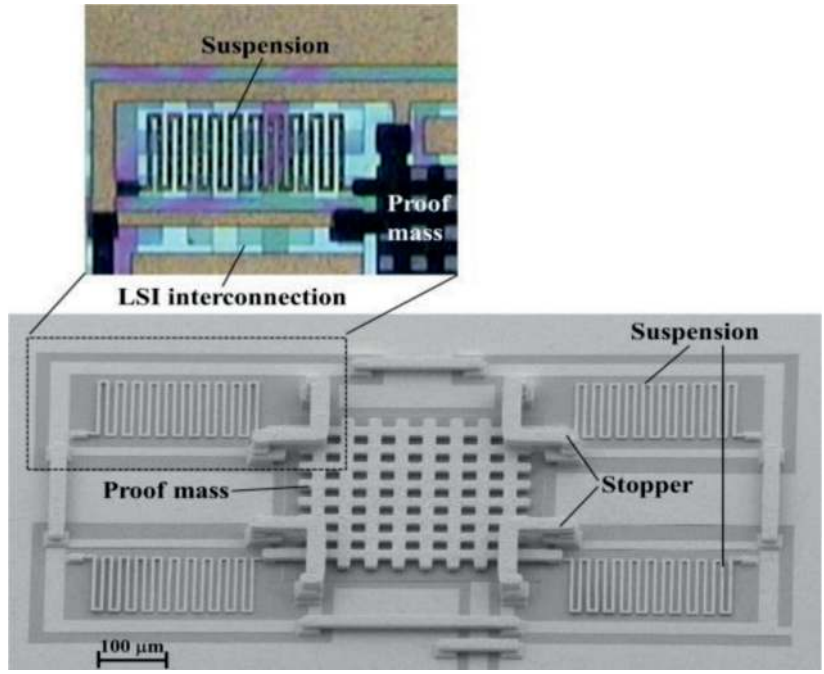

Figure 23.
A scanning electron microscopy (SEM) image.

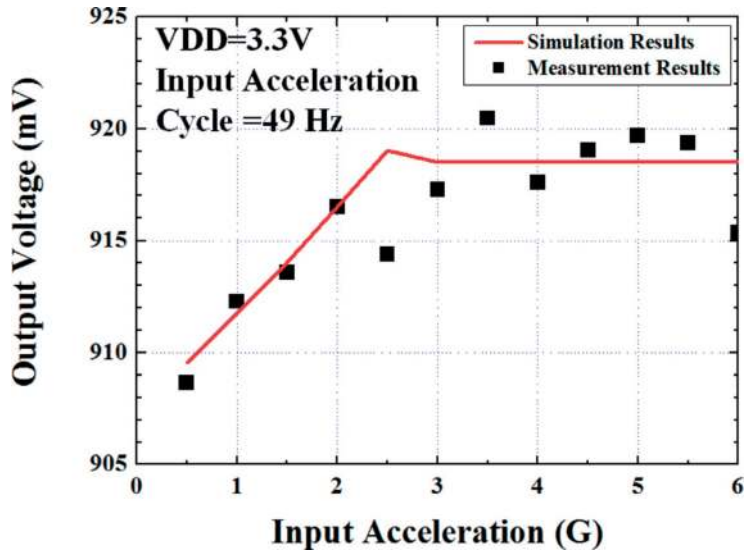

Figure 24.
The output voltage as a function of the input acceleration obtained by both experimental measurement and numerical simulation.

The simulation result was coincident with the experimental results for the input acceleration of 3 G or lower. For the input acceleration of 3 G or larger, notable deviations were observed in the experimental result possibly due to excess mechanical motion of the proof mass. The result suggested that fabricated capacitive CMOS-MEMS sensor can detect the capacitance change of a single-axis MEMS accelerometer.

Therefore, it is confirmed that the validity of the simultaneous design of both MEMS and sensor circuit using multi-physics simulation environment with an equivalent circuit of the MEMS accelerometer was verified.

7. Conclusions

This chapter presented technical features and solutions to realize a high sensitive CMOS-MEMS accelerometer with gold proof mass. The multi-physics simulation platform for the design of the CMOS-MEMS device was developed to understand simultaneously both the mechanical and electrical behaviors of MEMS stacked on LSI. An equivalent circuit for the accelerometer module was built by an electrical circuit simulator.

MEMS accelerometer fabrication process was formed by the multi-layer metal technology, which consists of the gold electroplating and the sacrificial layer formation using the photo-sensitive polyimide film. We proposed a sensor structure for MEMS accelerometers. The measured characteristics of the developed accelerometer were in good agreement with the designed values, and the actual Brownian noise was estimated to be below the target of 100 μG/(Hz)$^{1/2}$. Moreover, the experimental results showed that the Brownian noise of the sub-1G MEMS accelerometer could achieve 780 nG/(Hz)$^{1/2}$. We also proposed an arrayed accelerometer device with a wide range of detection between 1 and 20 G. An arrayed accelerometer was successfully developed in a single chip of 4×4 mm^2 in area by electroplated gold. The experimental results suggested that a wide detection range of acceleration has been achieved.

The proposed sensor LSI was fabricated by a 0.35-μm CMOS process and the MEMS accelerometer was implemented onto the LSI. The measured characteristics of the capacitive CMOS-MEMS accelerometer showed a good agreement with the simulation results. Thus, the validity of our multi-physics simulation was verified.

In conclusion, it is confirmed that the multi-physics simulation platform and the multi-layer metal technology for the CMOS-MEMS device will open the way to the future of nano-gravity sensing technology.

Acknowledgements

The authors would like to thank S. Iida, M. Yano, T. Safu, and K. Kudo with NTT-AT for technical discussions.

This work was supported by JST CREST Grant Number JPMJCR1433 and by the Grant-in-Aid for Scientific Research (B) (No. 23360149) of the Japan Society for the Promotion of Science (JSPS).

Conflicts of interest

I confirm there are no conflicts of interest.

DOI: http://dx.doi.org/10.5772/intechopen.81832

Author details

Katsuyuki Machida[1*], Toshifumi Konishi[2], Daisuke Yamane[1], Hiroshi Toshiyoshi[3] and Hiroyuki Ito[1]

1 Tokyo Institute of Technology, Yokohama, Kanagawa, Japan

2 NTT Advanced Technology Corporation, Atsugi, Kanagawa, Japan

3 RCAST, The University of Tokyo, Tokyo, Japan

*Address all correspondence to: machida.k.ad@m.titech.ac.jp

References

[1] Seidel H, Riedel H, Kolbeck R, Mück G, Kupke W, Königer M. Capacitive silicon accelerometer with highly symmetrical design. Sensors and Actuators A. 1990;**21**:312

[2] Henrion W, DiSanza L, Lp M, Terry S, Jerman H. Wide dynamic range direct digital accelerometer. In: IEEE 4th Solid-State Sensor and Actuator Workshop Technical Digest. 1990. p. 153

[3] Yun W, Howe T, Gray PR. Surface micromachined digitally force balanced accelerometer with integrated CMOS detection circuitry. In: IEEE 5th Solid-State Sensor and Actuator Workshop Technical Digest. 1992. p. 126

[4] Ohtsuki Y, Fuda Y, Yoshida T. High-sensitivity accelerometer using multilayer piezoelectric ceramics. Japanese Journal of Applied Physics. 1993;**32**:4209

[5] Ha B, Oh Y, Song C. A capacitive silicon microaccelerometer with force-balancing electrodes. Japanese Journal of Applied Physics. 1998;**37**:7052

[6] Kim S, Yee Y, Kim H, Chun K, Hong I, Lee J. A complementary metal oxide semiconductor (CMOS) compatible capacitive silicon accelerometer with polysilicon rib-style flexures. Japanese Journal of Applied Physics. 1998;**37**:7093

[7] Sim J-H, Lee J-H. A piezoresistive silicon accelerometer using porous silicon micromachining and flip-chip bonding. Japanese Journal of Applied Physics. 1999;**38**:1915

[8] Lee KI, Takao H, Sawada K, Ishida M. Analysis of thermal drift of a constant temperature control type three-axis accelerometer for high temperatures. IEEJ Transactions on Sensors and Micromachines. 2003;**123**:583

[9] Speller KE, Yu D. A low noise MEMS accelerometer for unattended ground sensor application. In: Proceedings of the SPIE Unattended/Unmanned Ground, Ocean, and Air Sensor Technologies and Applications VI. Vol. 5417. 2004. p. 63

[10] Okada H, Kobayashi T, Masuda T, Itoh T. Ultra-low power event-driven wireless sensor node using piezoelectric accelerometer for health monitoring. Japanese Journal of Applied Physics. 2009;**48**:070222

[11] Milligan D, Homeijer B, Walmsley R. An ultra-low noise MEMS accelerometer for seismic imaging. In: Proceedings of IEEE Sensors 2011; 28-31 October 2011; Limerick, Ireland. New Jersey: IEEE; 2012

[12] Abdolvand R, Amini B, Ayazi F. Sub-micro-gravity in-plane accelerometers with reduced capacitive gaps and extra seismic mass. Journal of Microelectromechanical Systems. 2007; **16**:1036-1043. DOI: 10.1109/JMEMS.2007.900879

[13] Dong Y, Kraft M, Redman-White W. Higher order noise-shaping filters for high-performance micromachined accelerometers. IEEE Transactions on Instrumentation and Measurement. 2007;**56**:1666-1674. DOI: 10.1109/TIM.2007.904477

[14] Monajemi P, Ayazi F. Design optimization and implementation of a microgravity capacitive HARPSS accelerometer. IEEE Sensors Journal. 2006;**6**:39-46. DOI: 10.1109/JSEN.2005.854134

[15] Chae J, Kulah H, Najafi K. An in-plane high-sensitivity, low-noise micro-g silicon accelerometer with CMOS readout circuitry. Journal of Microelectromechanical Systems. 2004;

13:628-635. DOI: 10.1109/JMEMS.2004.832653

[16] Yazdi N, Najafi K, Salian A. A high-sensitivity silicon accelerometer with a folded-electrode structure. Journal of Microelectromechanical Systems. 2003; **12**:479-486. DOI: 10.1109/JMEMS.2003.815837

[17] Kulah H, Chae J, Yazdi N, Najafi K. A multi-step electromechanical ΣΔ converter for micro-g capacitive accelerometers. In: Proceedings of IEEE International Solid-State Circuits Conference 2013; 13 February 2004; San Francisco, CA, USA. New Jersey: IEEE; 2004

[18] Yazdi Y, Najafi K. An all-silicon single-wafer micro-g accelerometer with a combined surface and bulk micromachining process. Journal of Microelectromechanical Systems. 2000; **9**:544-550. DOI: 10.1109/84.896777

[19] Lemkin M, Boser B. A three-axis micromachined accelerometer with a CMOS position-sense interface and digital offset-trim electronics. IEEE Journal of Solid-State Circuits. 1999;**34**: 456-468. DOI: 10.1109/4.753678

[20] Lu C, Lemkin M, Boser B. A monolithic surface micromachined accelerometer with digital output. IEEE Journal of Solid-State Circuits. 1995;**30**: 1367-1373. DOI: 10.1109/4.482163

[21] Smith T, Nys O, Chevroulet M, DeCoulon Y, Degrauwe M. A multi-step electromechanical /spl Sigma//spl Delta/ converter for micro-g capacitive accelerometers. In: Proceedings of IEEE International Solid-State Circuits Conference 1994; 16-18 February 1994; San Francisco, CA, USA. New Jersey: IEEE; 2002. pp. 160-161

[22] Analog Devices, ADXL50 [Internet]. Available from: http://www.analog.com/media/en/technical-documentation/obsolete-data-sheets/2044696ADXL50.pdf [Accessed: 28-08-2018]

[23] Yamane D, Konishi T, Matsushima T, Machida K, Toshiyoshi H, Masu K. Design of sub-1g microelectromechanical systems accelerometers. Applied Physics Letters. 2014;**104**(7):074102. DOI: 10.1063/1.4865377

[24] Yamane D, Konishi T, Matsushima T, Motohashi G, Kagaya K, Ito H, et al. An arrayed MEMS accelerometer with a wide range of detection. In: Transducers 2013; Spain. 2013. p. 22

[25] Konishi T, Yamane D, Matsushima T, Motohashi G, Kagaya K, Ito H, et al. Novel sensor structure and its evaluation for integrated complementary metal oxide semiconductor microelectromechanical systems accelerometer. Japanese Journal of Applied Physics. 2013;**52**: 06GL04

[26] Machida K, Shigematsu S, Morimura H, Tanabe Y, Sato N, Shimoyama N, et al. A novel semiconductor capacitive sensor for a single-chip fingerprint sensor/identifier. IEEE Transactions on Electron Devices. 2001;**48**:2273

[27] Machida K, Morimura H. Integrated CMOS-MEMS technology and its application. In: SSDM 2010; 24 September 2010; Tokyo. 2010. p. 818

[28] Toshiyoshi H, Konishi T, Machida K, Masu K. A multi-physics simulation technique for integrated MEMS. In: IEDM 2012; USA. 2012. p. 6.3.1

[29] Konishi T, Machida K, Maruyama S, Mita M, Masu K, Toshiyoshi H. A single-platform simulation and design technique for CMOS-MEMS based on a circuit simulator with hardware description language. IEEE/ASME:

Journal of Microelectromechanical Systems. 2013;**22**(3):755

[30] Konishi T, Yamane D, Matsushima T, Maruyama S, Kagaya K, Ito H, et al. Novel sensor circuits design using multi-physics simulation for CMOS-MEMS technology. In: SSDM 2013; 24-27 September 2013; Fukuoka, Japan. 2013. p. 844

[31] Cadence Design Systems, Inc. Available from: http://www.cadence.com/products/cic/pages/default.Aspx

[32] Qu H, Fnag D, Xie H. A monolithic CMOS-MEMS 3-axis accelerometer with a low-noise, low-power dual-chopper amplifier. IEEE Sensors Journal. 2008;**8**: 1511

[33] Chen J-Y, Liao LP, Chien HT, Lin CS, Hsu YW. Issues in Path Toward Low Cost Three-Axis Accelerometer for Low-g Application. In: Proceedings of the 4th International Microsystems, Packaging, Assembly and Circuits Technology Conference. 2009. p. 263

[34] Comi C, Corigliano A, Langfelder G, Longoni A, Tocchio A, Simoni B. A resonant microaccelerometer with high sensitivity operating in an oscillating circuit. IEEE Journal of Microelectromechanical Systems. 2010; **19**:1140

[35] Sato N, Morimura H, Shigematsu S, Yano M, Kudou K, Kamei T, et al. Force-sensing scheme for small mechanical signals in CMOS MEMS fingerprint sensor. Japanese Journal of Applied Physics. 2005;**44**:6481

[36] Kuwabara K, Urano M, Kodate J, Sato N, Morimura H, Sakata T, et al. Novel structure and fabrication process for integrated RF microelectormechanical-system technology. Japanese Journal of Applied Physics. 2006;**45**:6849

[37] Mitcheson PD, Yeatman EM, Rao GK, Holmes AS, Green TC. Energy harvesting from human and machine motion for wireless electronic devices. Proceedings of the IEEE. 2008;**96**:1457

[38] Kulahv H, Najafi K. Energy scavenging from low frequency vibrations by using frequency up conversion for wireless sensor applications. IEEE Sensors Journal. 2008;**8**(3):261-268

[39] Gray PR, Hurst PJ, Lewis SH, Meyer RG. Analysis and Design of Analog Integrated Circuits. 4th ed. New York: John Wiley & Sons, Inc.; 2001. p. 796

[40] Senturia SD. Microsystem Design. New York: Springer Science+Business Media, Inc.; 2001

[41] Jung WG. Op Amp Applications. Analog Devices, Inc; 2002. p. 1.83

[42] Kulah H, Chae J, Yazdi N, Najafi K. Noise analysis and characterization of a sigma-delta capacitive microaccelerometer. IEEE Journal of Solid-State Circuits. 2006;**41**(2):352-361

[43] Denison T, Consoer K, Santa W, Miesel K, Molnar G. A 2.2 microWatt, 95nV/rtHz, chopper-stabilized instrumentation amplifier for chronic measurement of ECG and EEG. In: Proceedings of the Instrumentation and Measurement Technology Conference. 2007. p. 1

[44] Chen J, Ni X, Mo B. A low noise CMOS charge sensitive preamplifier for MEMS capacitive accelerometer readout. In: Proceedings of the 7th International Conference on ASIC. 2007. p. 490